Supporting Information

Hexameric Silver(I) Pyrazolate: Synthesis, Structure and Isomerization

Xing-Pu Lv, Dong-Hui Wei and Guang Yang *

College of Chemistry and Molecular Engineering, Zhengzhou University, Zhengzhou 450001, China

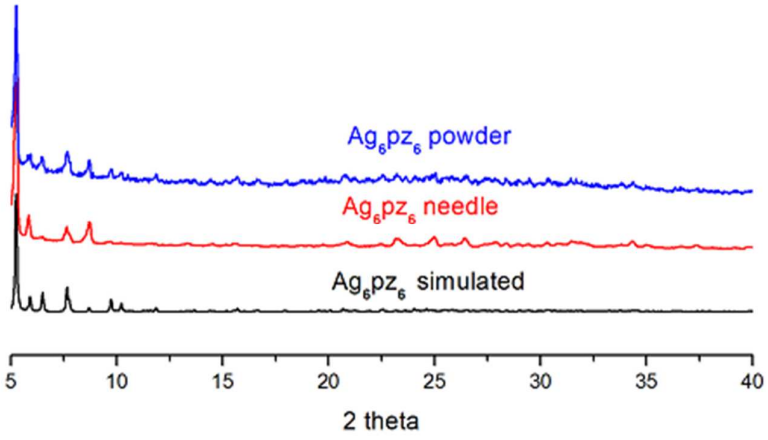

Figure S1. The XPRD patterns of the powdery product (blue line), the needles from solvothermal synthesis (red line) and that simulated from crystal data (black line). By comparison, it can be concluded that the product obtained by ambient synthesis is the needle polymorph of Ag_6pz_6.

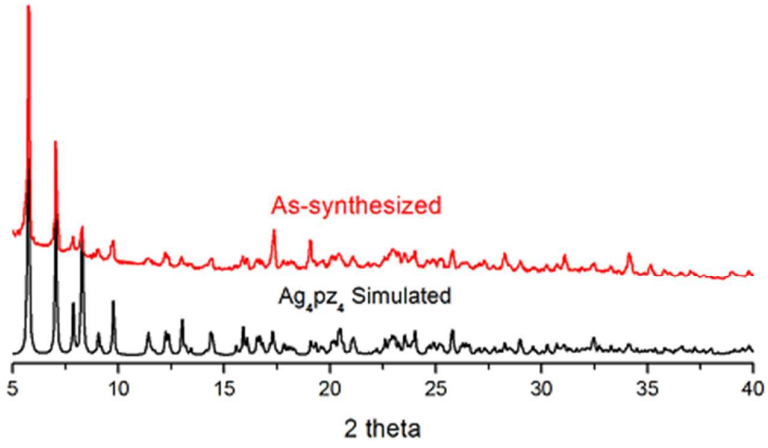

Figure S2. The XPRD pattern of the crystals obtained by recrystallization of Ag_6pz_6 from ether (red line) and that of Ag_4pz_4 simulated from crystal data. By comparison, it can be concluded that the hexameric Ag_6pz_6 has been converted to tetrameric Ag_4pz_4 *via* recrystallization.

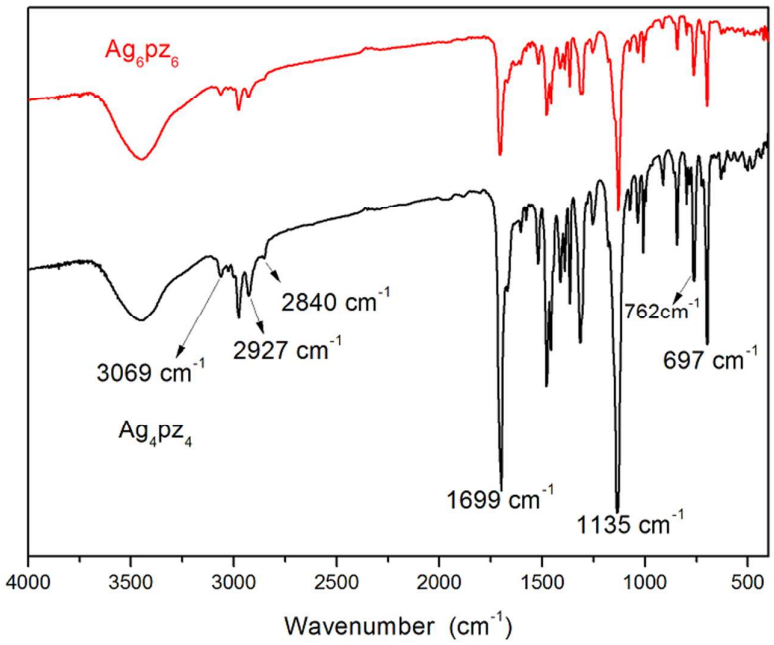

Figure S3. IR spectra of Ag_4pz_4 and Ag_6pz_6.

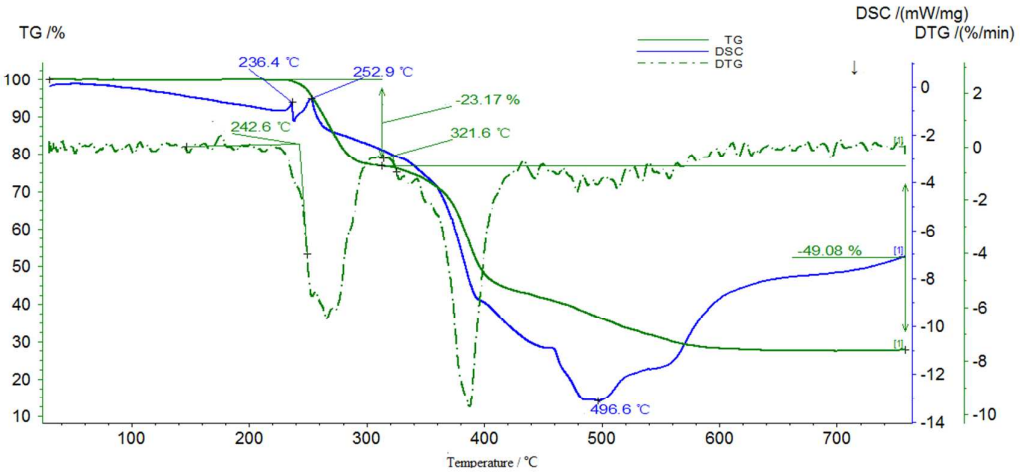

Figure S4. TG and DSC curves of Ag_6pz_6.

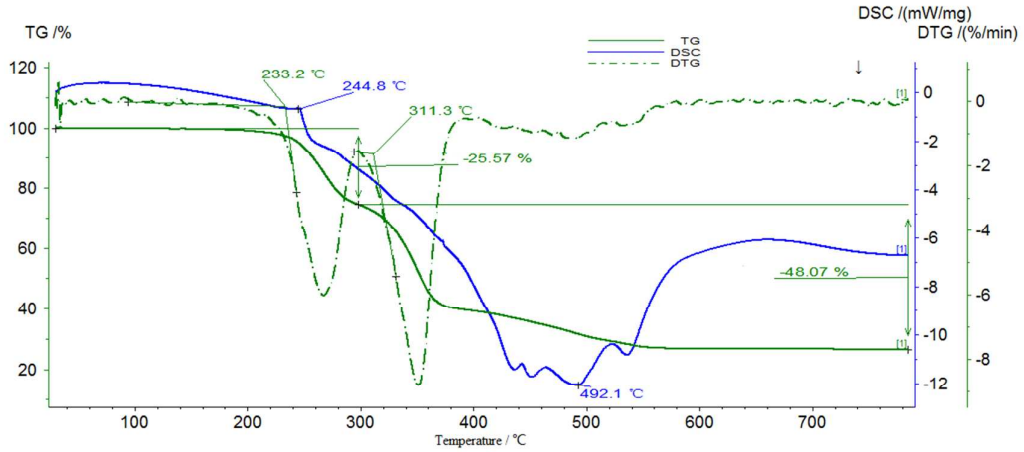

Figure S5. TG and DSC curves of Ag_4pz_4.

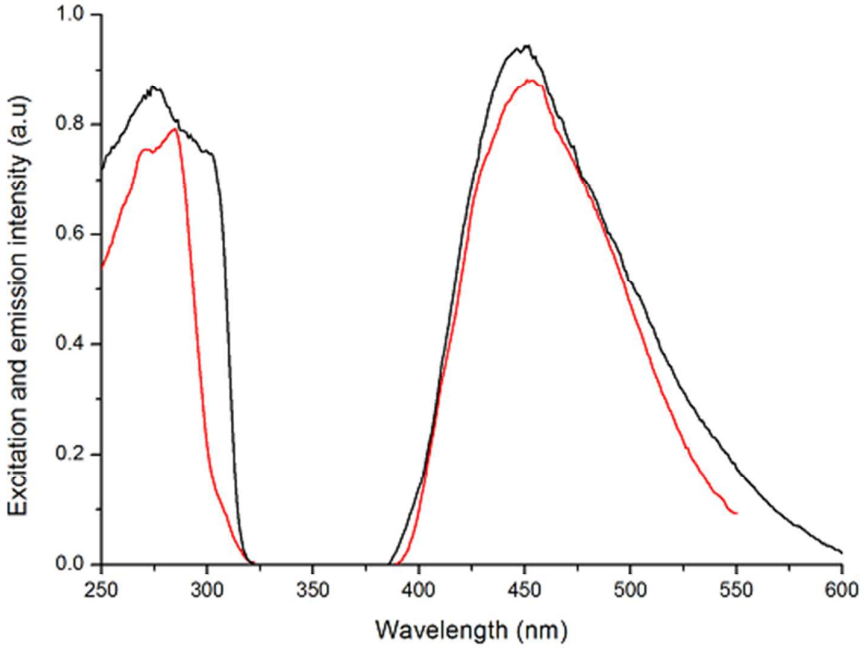

Figure S6. Solid state luminescent spectra of Ag_4pz_4 (red) and Ag_6pz_6 (black) at 83 K.

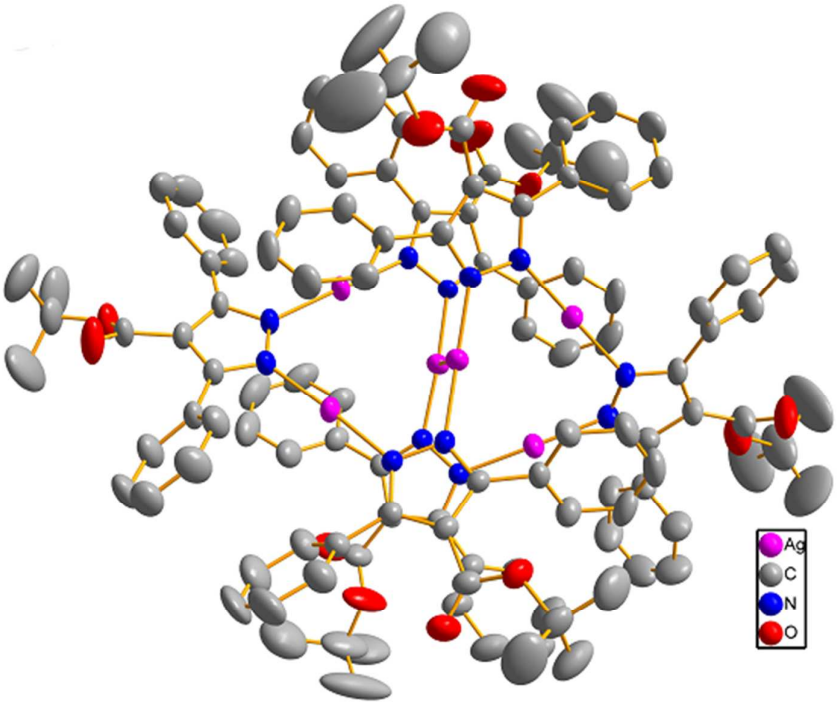

Figure S7. ORTEP diagram of the asymmetry unit of the block polymorph of Ag_6pz_6.

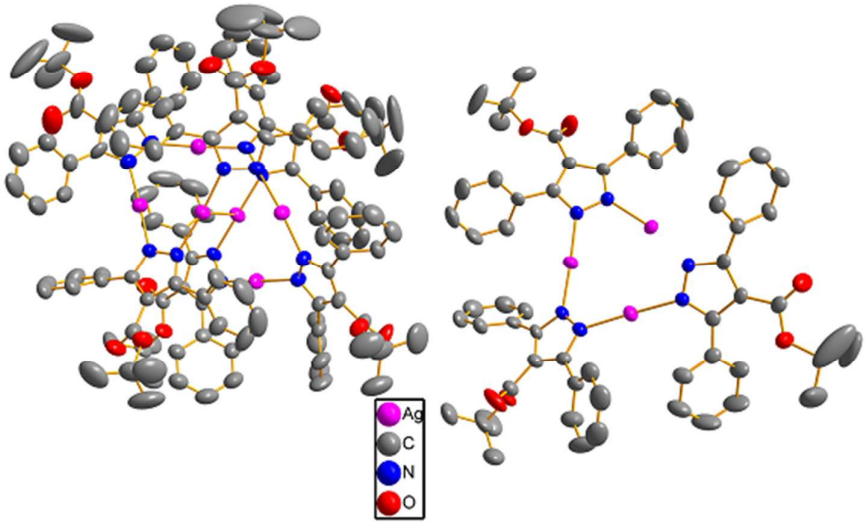

Figure S8. ORTEP diagram of the asymmetry unit of the needle polymorph of Ag_6pz_6.

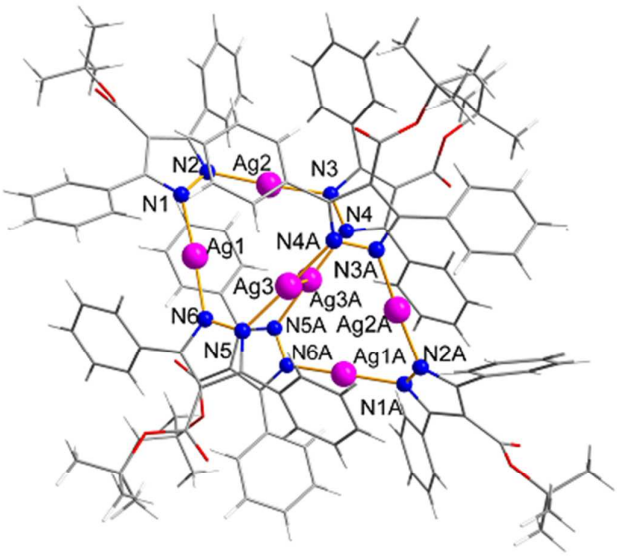

Figure S9. Ball-and-stick diagram of the Ag_6pz_6 molecule, which is found as half of the molecule in the asymmetric unit of the needle polymorph of Ag_6pz_6. Selected distances (Å): Ag-N, 2.0718(16)-2.0970(15); Ag1⋯Ag2 3.5666(3); Ag1⋯Ag3 4.2263(3); Ag1⋯Ag3A 3.4360(2); Ag2⋯Ag3 3.5256(2); Ag2-Ag3A 4.1887(2); Ag3⋯Ag3A 3.1995(3). Selected angles (°): N1-Ag1-N6 173.99(10); N2-Ag2-N3 176.74(9); N5A-Ag3-N4 174.57(9). Symmetry code: A) *-x, y, 1.5-z*.

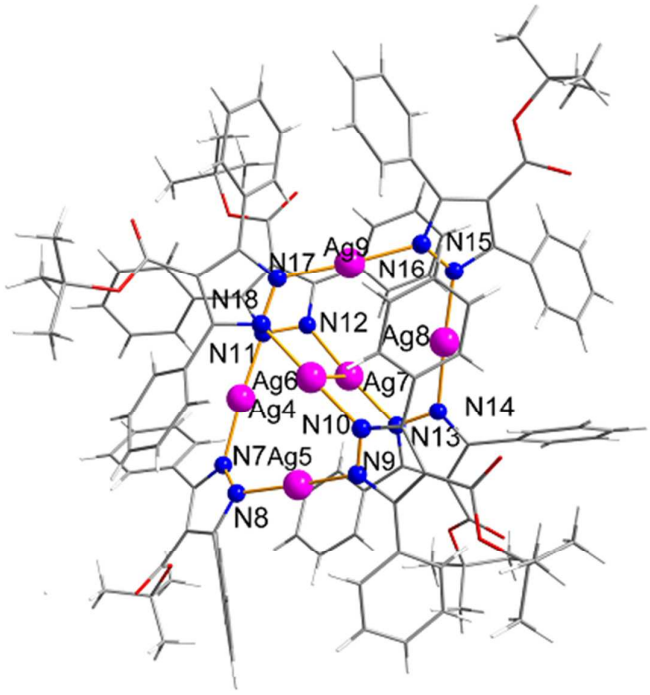

Figure S10. Ball-and-stick diagram of the Ag_6pz_6 molecule, which is found as one whole molecule in the asymmetric unit of the needle polymorph of Ag_6pz_6. Selected distances (Å): Ag-N, 2.0573(13)-2.0987(15); Ag4⋯Ag5 3.7401(3); Ag4⋯Ag6 3.9742(3); Ag4⋯Ag7 3.3113(3); Ag5⋯Ag6 3.2819(3); Ag5⋯Ag7 3.9923(3); Ag6⋯Ag7 3.2708(3); Ag6⋯Ag8 4.2822(3); Ag6⋯Ag9 3.4138(3); Ag7⋯Ag8 3.2362(3); Ag7⋯Ag9 4.1308(3); Ag8⋯Ag9 3.7162(3); Selected angles (°): N7-Ag4-N11 173.60(6); N8-Ag5-N9 172.15(6); N18-Ag6-N10 172.51(6); N12-Ag7-N13 172.40(6); N15-Ag8-N14 176.99(7); N17-Ag9-N16 176.87(7).

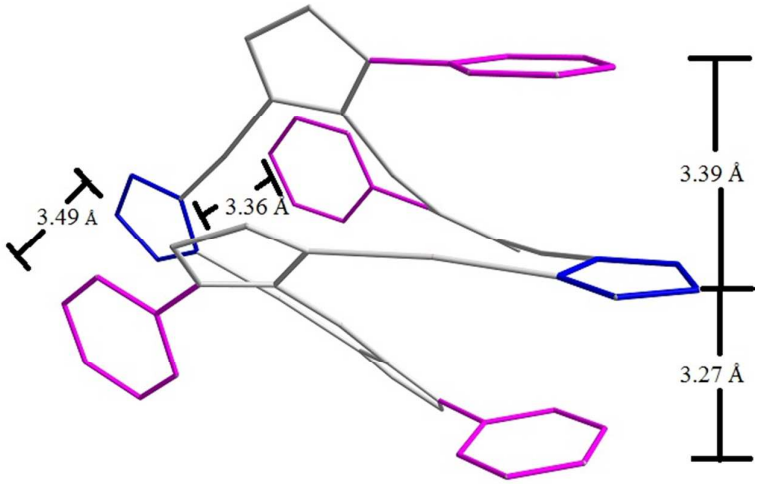

Figure S11. The triple-deck structural motifs in Ag_6pz_6, showing the face-to-face π–π stacking involving two endwise pyrazolyl rings, as complementary to Figure 2.

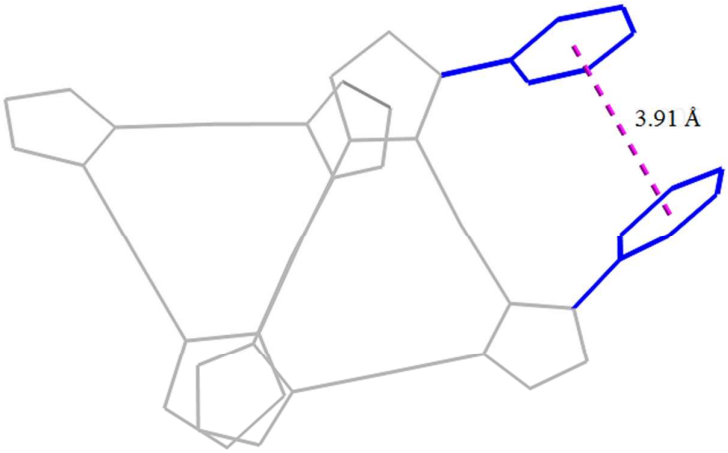

Figure S12. The intramolecular phenyl-phenyl stacking in Ag_6pz_6 (block polymorph).

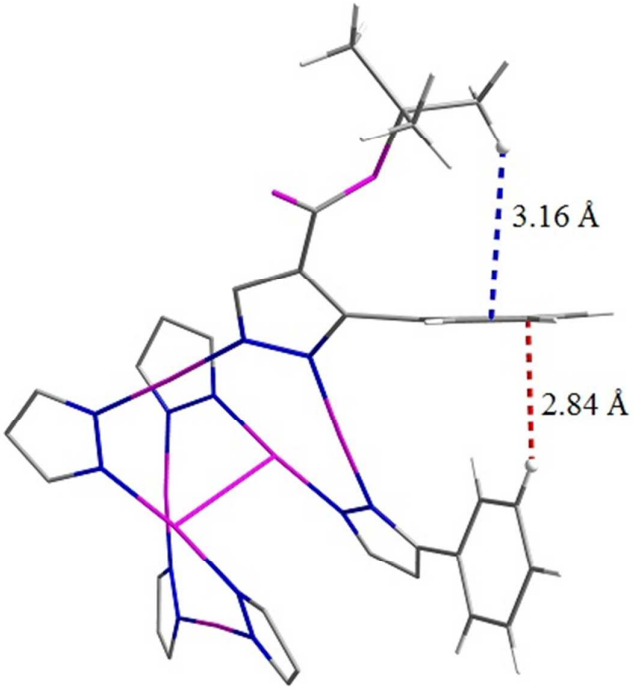

Figure S13. The intramolecular C–H···π interactions in Ag_6pz_6 (block polymorph).

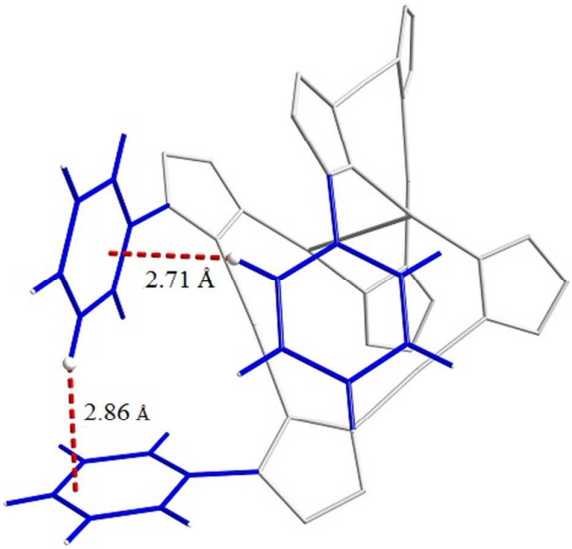

Figure S14. The C–H···π interactions involving three phenyl rings observed in Ag_6pz_6 (block polymorph).

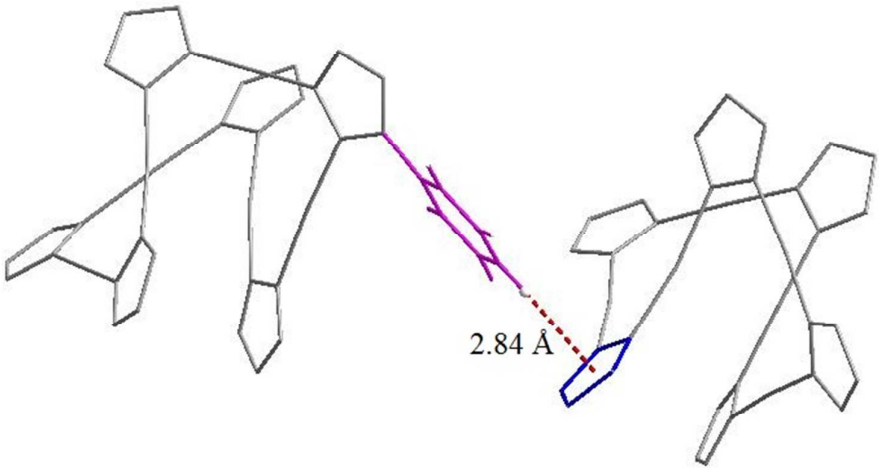

Figure S15. The intermolecular C–H···π interaction in Ag_6pz_6 (block polymorph).

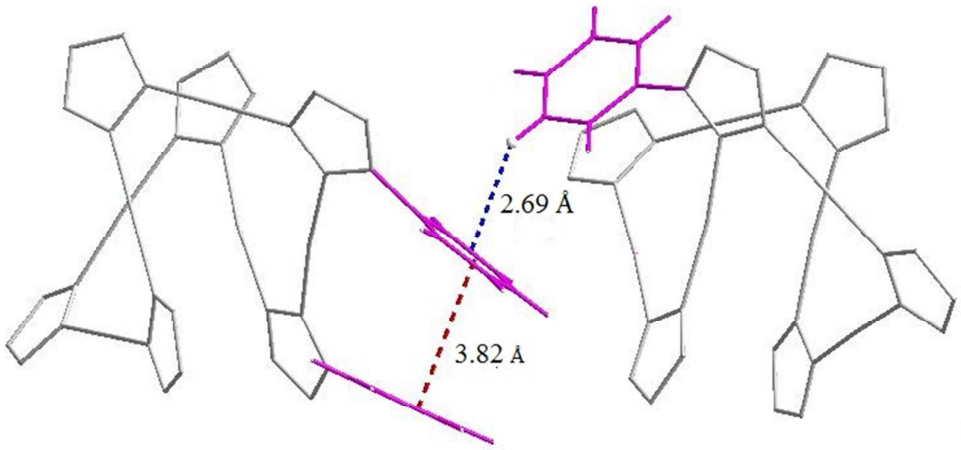

Figure S16. The intermolecular C–H···π interaction in Ag_6pz_6 (block polymorph).

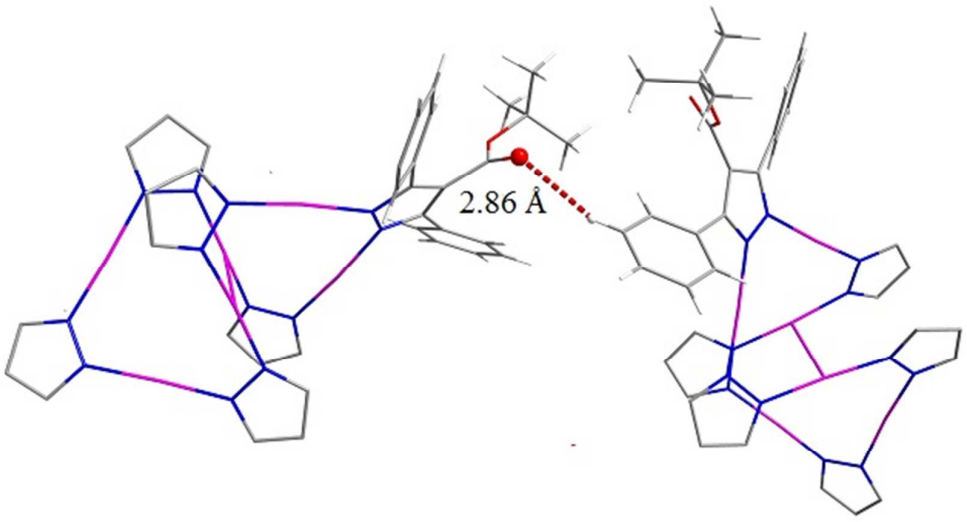

Figure S17. The intermolecular C-H···O hydrogen bond observed in Ag_6pz_6 (block polymorph).

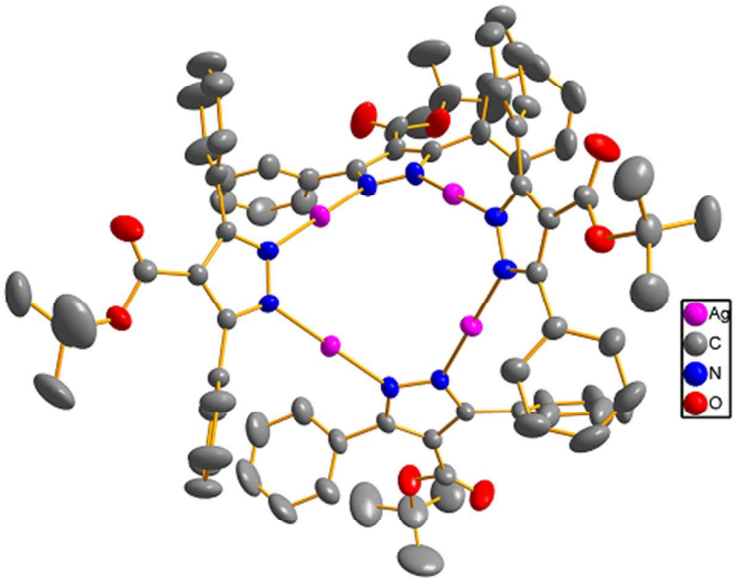

Figure S18. ORTEP diagram of the asymmetry unit of Ag_4pz_4.

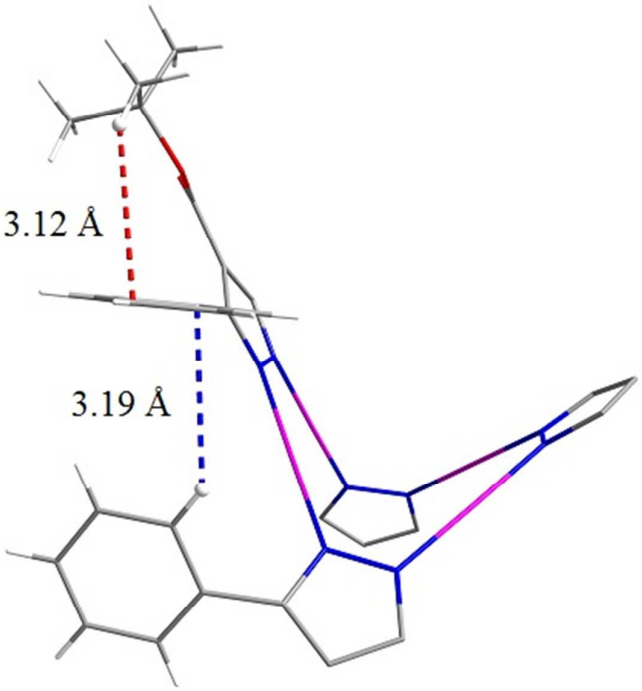

Figure S19. The intramolecular C–H···π interactions in Ag_4pz_4.

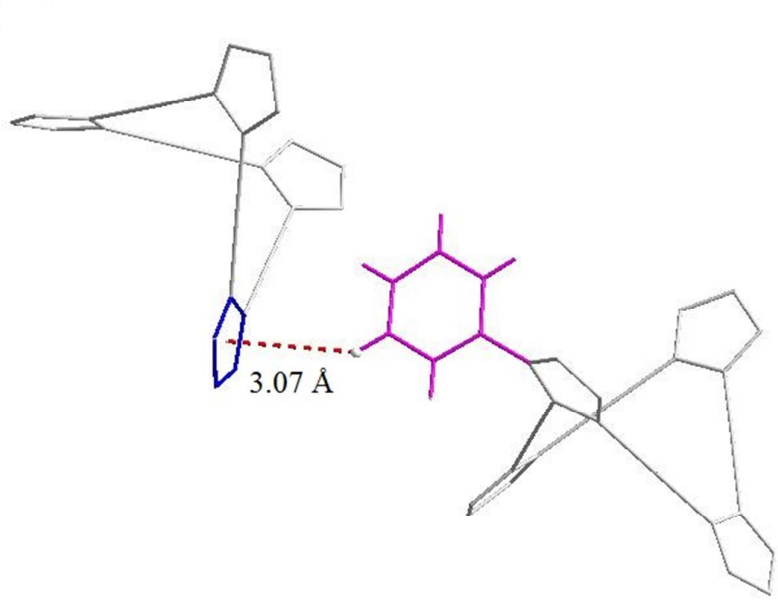

Figure S20. The intermolecular C–H···π interaction in Ag_4pz_4.

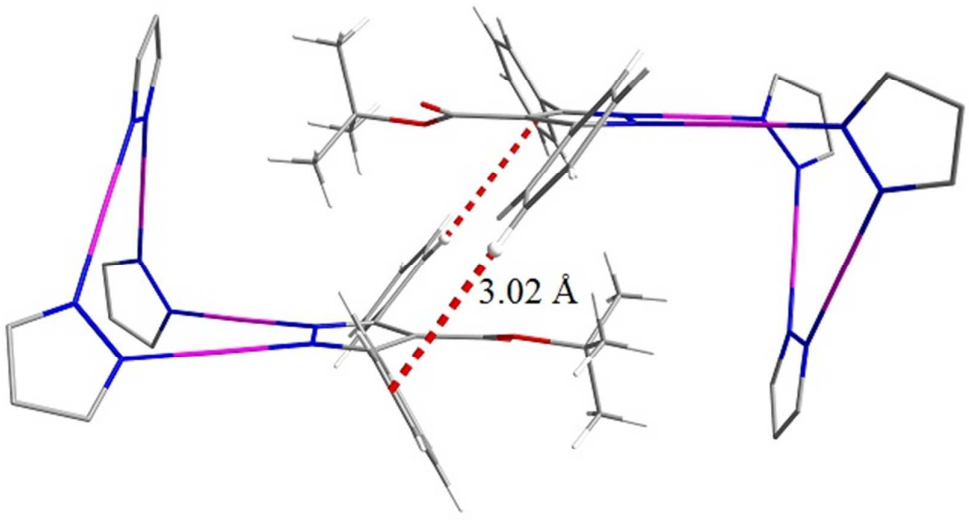

Figure S21. The C(Ph)-H···Ph interactions between a pair of neighboring Ag_4pz_4 molecules, as complementary to Figure 4.

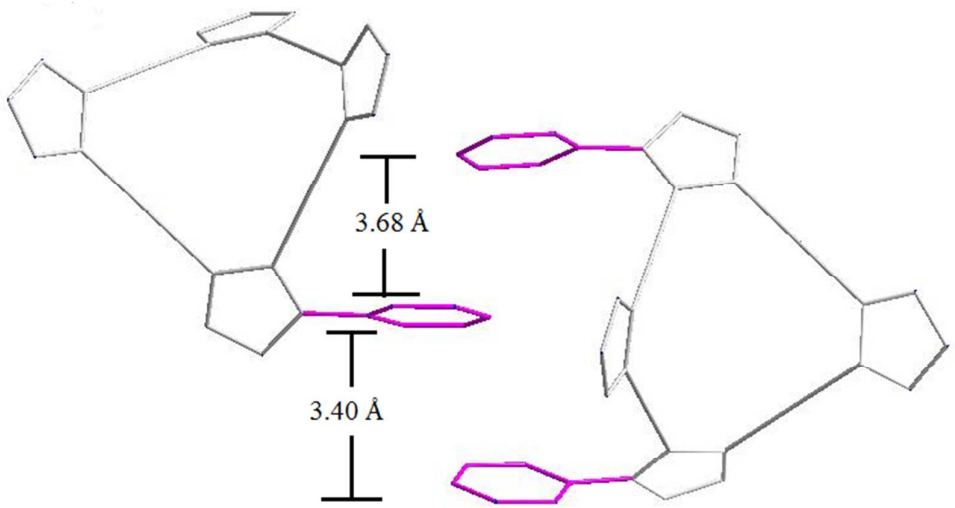

Figure S22. The intermolecular π–π stacking between a pair of neighboring Ag_4pz_4 molecules.

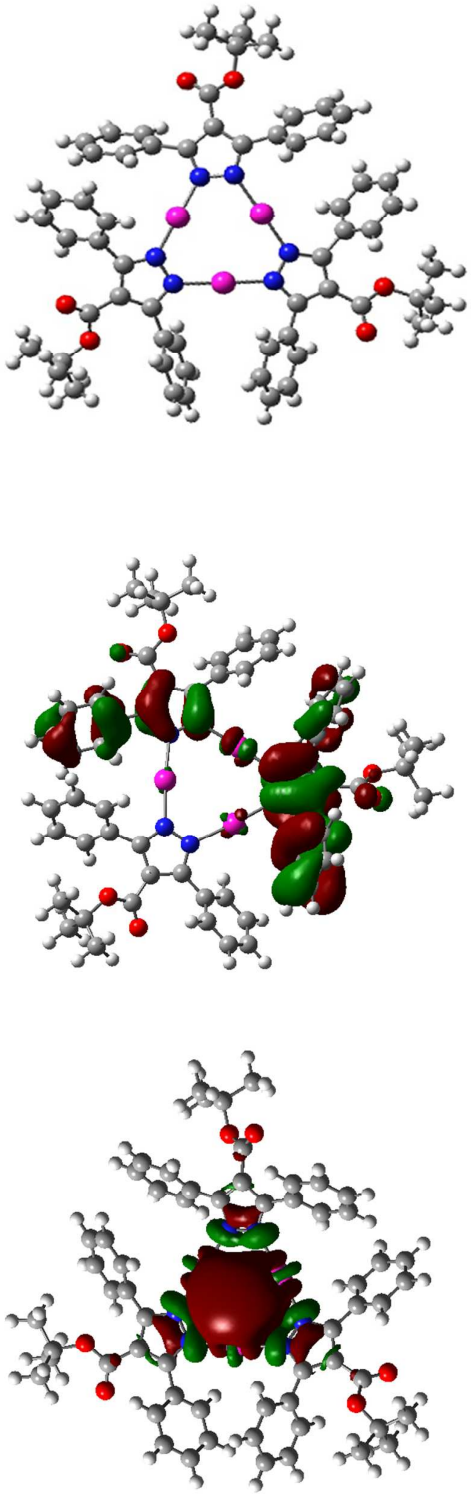

Figure S23. The optimized geometry, HOMO and LUMO of the hypothetic Ag_3pz_3 molecule.

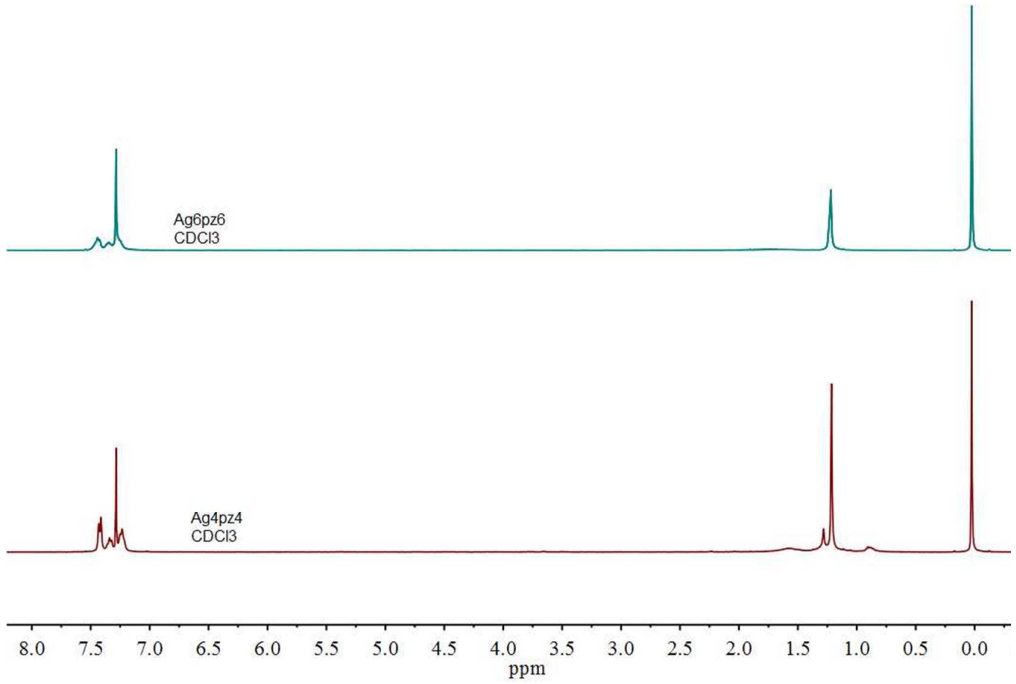

Figure S24. ^{1}H NMR spectra of Ag_4pz_4 and Ag_6pz_6 in $CDCl_3$ at 298 K.

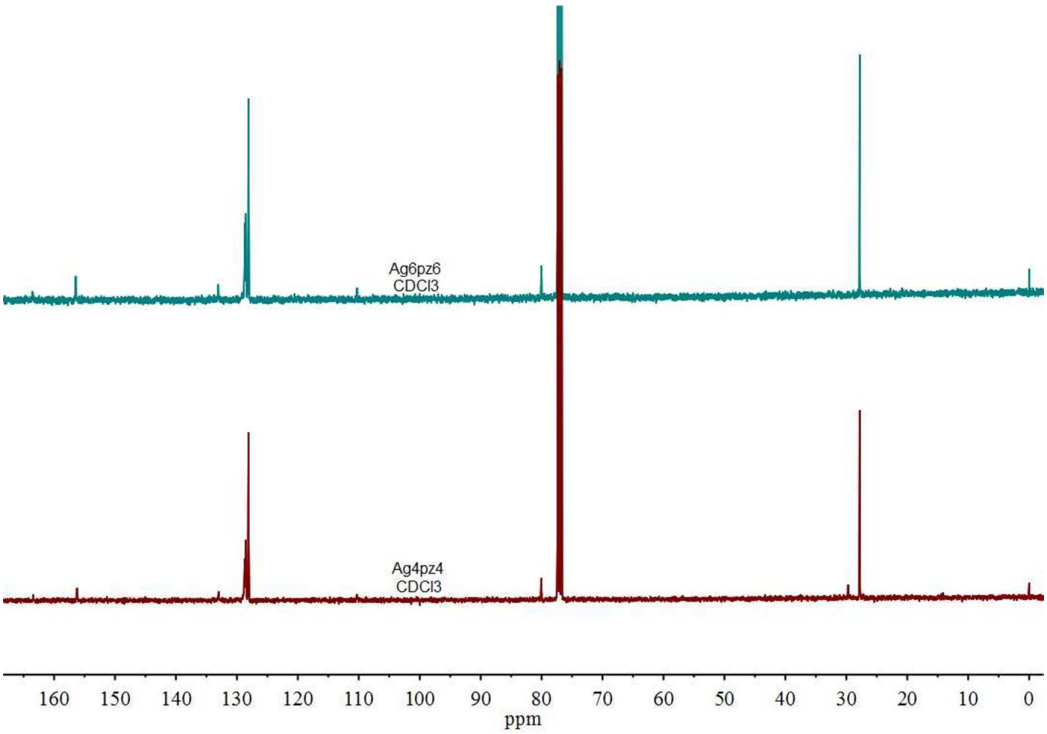

Figure S25. ^{13}C NMR spectra of Ag_4pz_4 and Ag_6pz_6 in $CDCl_3$ at 298 K.

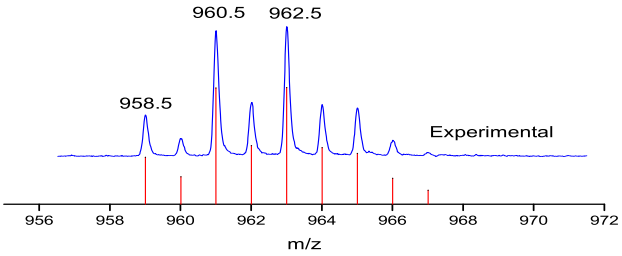

Figure S26. MALDI-TOF mass spectrum of $[Ag_3pz_2]^+$ with enlargement of the molecular ion peak (962.5 *m*/*z*) and its simulated isotopic pattern.

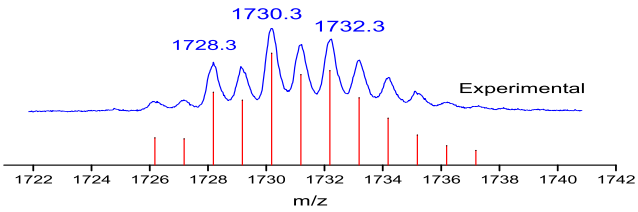

Figure S27. MALDI-TOF mass spectrum of $[Ag_4pz_4]+Na^+$ with enlargement of the molecular ion peak (1730.3 *m*/*z*) and its simulated isotopic pattern.

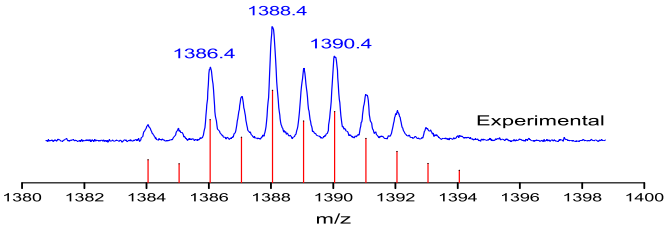

Figure S28. MALDI-TOF mass spectrum of $[Ag_4pz_3]^+$ with enlargement of the molecular ion peak (1388.4 *m*/*z*) and its simulated isotopic pattern.

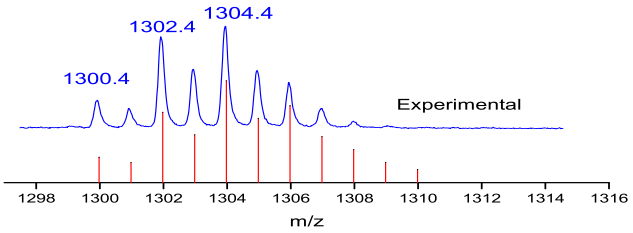

Figure S29. MALDI-TOF mass spectrum of $[Ag_4pz_2pz']^+$ with enlargement of the molecular ion peak(1304.4 *m*/*z*) and its simulated isotopic pattern.

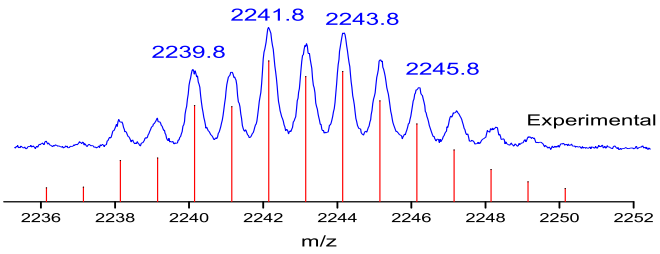

Figure S30. MALDI-TOF mass spectrum of $[Ag_6pz_5]^+$ with enlargement of the molecular ion peak (2241.8 *m*/*z*) and its simulated isotopic pattern.